Journal of Applied Physics

Anomalous Hall effect and magnetic properties of Fe_xPt_{100-x} alloys with strong spin-orbit interaction

Cite as: J. Appl. Phys. **122**, 033901 (2017); https://doi.org/10.1063/1.4994010
Submitted: 12 April 2017 • Accepted: 02 July 2017 • Published Online: 19 July 2017

Qiang Hao, Wenzhe Chen, Shutong Wang, et al.

AIP Publishing

Anomalous Hall effect and magnetic properties of Fe_xPt_{100-x} alloys with strong spin-orbit interaction

Qiang Hao, Wenzhe Chen, Shutong Wang, and Gang Xiao[a)]
Department of Physics, Brown University, Providence, Rhode Island 02912, USA

(Received 12 April 2017; accepted 2 July 2017; published online 19 July 2017)

We systematically study the magnetic properties, electron transport, and the anomalous Hall effect (AHE) in Fe_xPt_{100-x} solids over a wide composition range. These solids are characterized by strong spin-orbit interaction and enhanced magnetic moments from both elements. In our study, we vary the thickness and the composition of the thin films, the temperature of measurement, and the magnitude of the magnetic field in various directions. We have determined the Hall angle, the spin diffusion length, and the electron mean free path in this alloy system. The AHE is more than 3 orders of magnitude larger than the normal Hall effect, making Fe_xPt_{100-x} a good candidate for spintronic applications. The Hall angle determined in the Fe_xPt_{100-x} solids is comparable to that in pure Pt. From the analysis on the correlation between the AHE and electron transport, we find that the AHE is dominated by both the intrinsic Karplus-Luttinger (Berry phase) mechanism and the extrinsic side-jump mechanism. *Published by AIP Publishing*. [http://dx.doi.org/10.1063/1.4994010]

I. INTRODUCTION

In solids with high atomic numbers, spin-orbit interactions (SOIs) can play an important role in electron transport phenomena such as the Hall effect.[1] A magnetic metal often exhibits an anomalous Hall effect (AHE)[1] with a strength exceeding the normal Hall effect due to the Lorentz force. Recently, the giant spin Hall effect (GSHE)[2–6] was discovered in certain non-magnetic metals, in which a charge current is converted into a spin current with a large efficiency. The mechanism for the AHE could be either intrinsic, if created by the Berry phase curvature,[1,7,8] or extrinsic, if due to skew scattering or side jumping off SOI disorder sites.[1] On the other hand, the mechanism for GSHE is not well understood, although the extrinsic mechanism certainly plays a role. It is not clear if there is a dominant intrinsic mechanism behind the GSHE. The physics of the AHE and the GSHE significantly overlaps[1,6,9] except that the AHE creates a spin imbalance in the electrons, while the GSHE creates a positional bias of spin states but retains the overall equal ratio of spin up and down states. In the study of the GSHE, one often uses the AHE to sense the conversion of charge current to spin current.[4,6] Both the AHE and the GSHE can be used as a source of spin current.[4,6,9] There has been growing interest in both effects fundamentally and in spintronics applications such as magnetic sensors, magnetic random access memories, and spin logic devices.[1–6,9–15]

The search for a very large AHE has been going on for a long time.[10–15] Magnetic sensors based on the AHE have many advantages in sensing linearity, broad frequency response, and ease of fabrication.[10–13,15] Solids with a large AHE offer a good platform to study the intrinsic mechanism in addition to the extrinsic mechanism of the side jump.[1,8] Among all the materials exhibiting the AHE, Fe_xPt_{100-x} has received much attention[10,11,13] for the greater strength of the effect in the system. The alloy system offers a wide range of material tunability in composition which aids the study of the correlation between the transverse and longitudinal resistivities. However, there is a lack of a systematic study on the magnetic properties, transport, and the AHE versus composition, temperature, and material parameters such as thin film thickness. Fe_xPt_{100-x} alloys are ferromagnetic with strong magnetic anisotropy and corrosion resistance.[16,17] In their equilibrium phases,[18] $Fe_{25}Pt_{75}$ and $Fe_{75}Pt_{25}$ have the face-centered-cubic (fcc) $L1_2$ super-structures,[17] and $Fe_{50}Pt_{50}$ has the face-centered-tetragonal (fct) $L1_0$ super-structure (magnetization 1140 emu/cm^3).[17] Due to these properties, these atomically ordered solids have been extensively studied for potential use in high density magnetic recording media[19] and shape-memory applications.[20] In thin film preparation, high substrate temperatures are required to obtain these superstructures. If deposited under ambient conditions, Fe_xPt_{100-x} thin films form the fcc $A1$-type solid solution[21] in which the atomic sites are randomly occupied by Fe and Pt with a lattice constant of 0.386 nm for $Fe_{25}Pt_{75}$ and 0.381 nm for $Fe_{50}Pt_{50}$.[17]

In this work, we systematically study the magnetic properties, electron transport, and the AHE of the solid solution phase of Fe_xPt_{100-x} thin films with high resistivities and strong SOI. These characteristics lead to a very large AHE with a large Hall angle. Another advantage of this system is that the Fe concentration can be varied continuously from 0 to 100 at. % without any phase separation.[18] In this work, we focus on the Fe concentration range from 29 to 47%, thin-film thickness from 1.8 to 30 nm, and measurement temperature range from 2 K to 300 K. These variables have allowed us to investigate the Hall angle and correlation between the AHE and resistivities, providing elucidation on the mechanism for the large AHE observed in this system. We will present magnetic properties and key parameters such as electron mean-free path and spin diffusions length in this alloy system, as a result of thickness dependence studies.

[a)]Electronic mail: Gang_Xiao@Brown.edu

II. EXPERIMENT

We use a homemade high vacuum magnetron sputtering system to fabricate the Fe_xPt_{100-x} alloys. The base pressure of the vacuum chamber is about 1×10^{-7} Torr, and the Ar sputtering pressure is ~2 mTorr. Two 5 cm-diameter magnetron guns are loaded individually with Fe (purity 99.9%) and Pt (purity 99.9%) targets. The guns use NdFeB permanent magnet rings to generate a magnetic field near the surfaces of the targets. The target-substrate distance is 9 cm. The face-down substrate is a thermally oxidized single crystal Si wafer with a diameter of 5 cm. During deposition, which occurs under an ambient condition, we maintain constant sputtering rates of Fe and Pt and alternate the position of a substrate rapidly across the Fe and Pt beams until the intended film thickness is reached. By controlling the relative sputtering rates between the two targets, we can obtain any particular composition of Fe_xPt_{100-x} alloy.[22] Prior to deposition, the Si wafer is patterned with photoresist to define multiple standard Hall bars ($20 \times 55\ \mu m^2$ in area) using photolithography. After deposition, we use a lift-off process to obtain patterned Fe_xPt_{100-x} Hall bars for electron transport, magnetotransport, and magnetization measurements, which are carried out using the Quantum Design® Physical Property Measurement System (PPMS) over a temperature range of 2 to 300 K.

III. RESULTS AND DISCUSSION

The X-ray Diffraction (XRD) results of Fe_xPt_{100-x} thin films in the composition range of 29% to 47% are shown in Fig. 1. Only the (111) and (222) peaks of the face-centered-cubic (fcc) structure are observed in a representative 30 nm-thick $Fe_{29}Pt_{71}$ film. All the other listed Fe_xPt_{100-x} films with different compositions show the same fcc A1-type structure without secondary phase as in Fig. 1(a). The XRD pattern details are shown in Figs. 1(b) and 1(c). Therefore, the observed XRD pattern can verify the *A*1-type Fe_xPt_{100-x} structure.[22]

We study the magnetic properties and magnetotransport of the Fe_xPt_{100-x} thin films within the composition range of x = 29–47 at. %, where the system exhibits a very large AHE. Additionally, we vary the thickness from 3 to 30 nm, which is found to have a strong impact on the magnetotransport. All our samples are ferromagnetic at room temperature. The study of magnetic properties is necessary to investigate the AHE which is discussed later. Figure 2 shows magnetization (M) curves as functions of an in-plane magnetic field for a representative 30 nm-thick $Fe_{29}Pt_{71}$ film in the temperature range of 2 to 300 K. All other samples show similar behavior as shown in Fig. 2. M is easily saturated with a low field as the magnetically A1 soft phase, due to the in-plane magnetic shape anisotropy. By extrapolating M in the saturation region to the zero field, we obtain the spontaneous magnetization M_S(T) at a particular temperature.

Figure 3(a) shows the relationship between M_S(T) and $T^{3/2}$ ($2 \leq T \leq 300$ K) for a series of 30 nm-thick Fe_xPt_{100-x} thin films (x = 29, 35, 41, and 47). As can be seen, all samples follow Bloch's law of thermal spin-wave excitation[23,24]

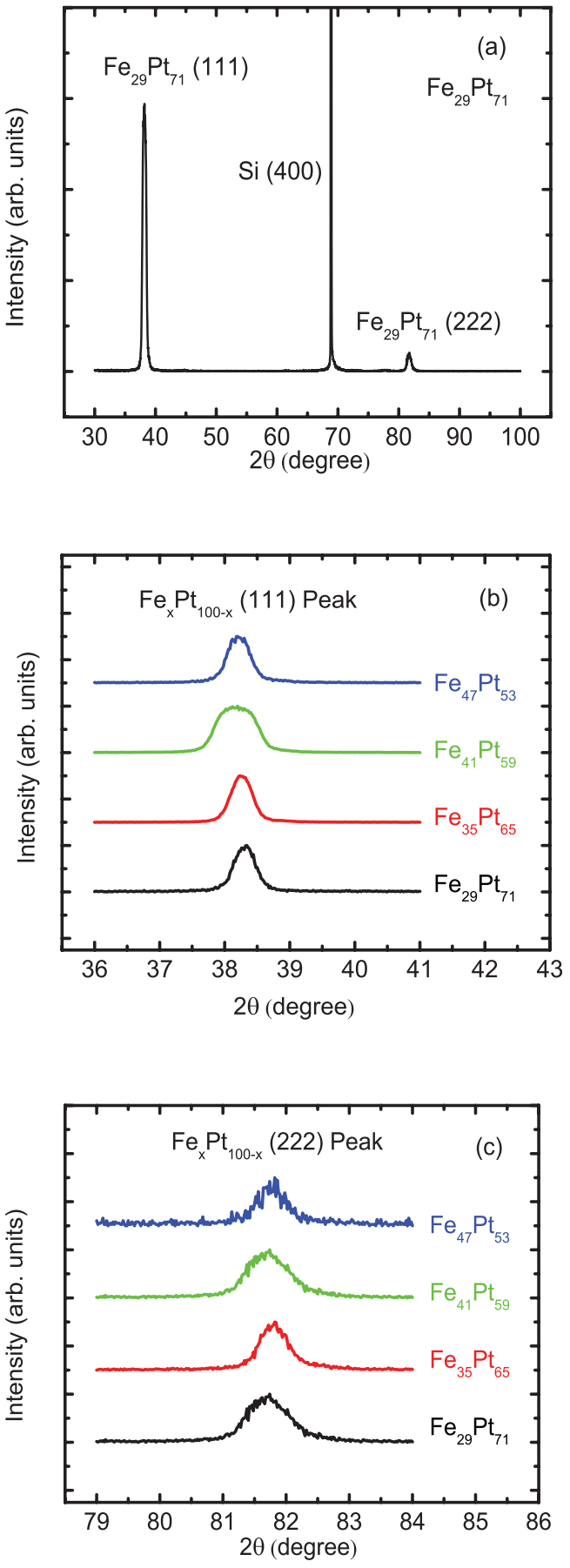

FIG. 1. (a) X-ray diffraction patterns of $Fe_{29}Pt_{71}$ film. (b) and (c) The details of XRD pattern (111) and (222) peaks for all the listed samples.

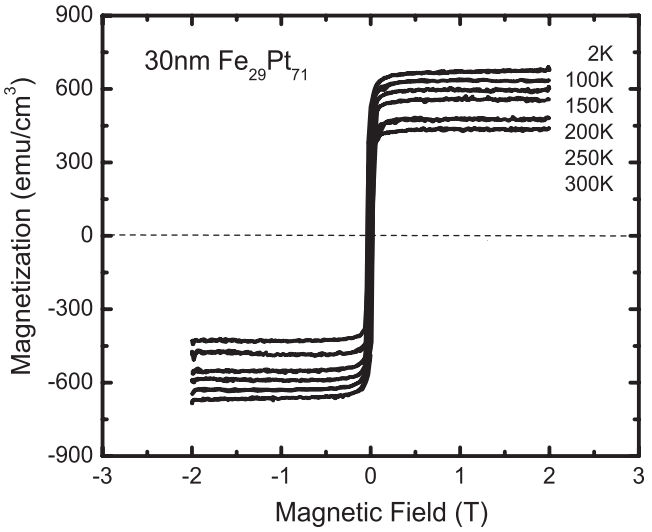

FIG. 2. Magnetization versus field curves of the 30 nm-thick $Fe_{29}Pt_{71}$ film at various temperatures (2–300 K). The magnetic field is applied in the plane of the film.

$$M_S(T) = M_S(0)\left(1 - AT^{\frac{3}{2}}\right). \quad (1)$$

Figure 3(b) shows the Fe concentration dependence of M_S at 2 and 300 K. M_S increases steadily with the Fe concentration and reaches a plateau of about 930 emu/cm^3 at 2 K around x = 41 to 45. Based on the data of M_S, we calculate the Fe effective magnetic moment μ^*_{Fe}, which is also shown in Fig. 3(b). The value of μ^*_{Fe} assumes that both the Fe moment and the induced Pt moment reside on the Fe sites. For $Fe_{29}Pt_{71}$, μ^*_{Fe} is 3.5 μ_B. This value is consistent with the idea that the total magnetic moment is a mixture of $\mu_{Fe} = 2.75$ μ_B and $\mu_{Pt} = 0.3$ μ_B, as proposed for the Fe-Pt random alloys.[25] For $A1$ $Fe_{25}Pt_{75}$, moment mixing would lead to the prediction of μ^*_{Fe}=3.7 μ_B. As a comparison, the magnetic structure of the $L1_2$ super-structure of $Fe_{25}Pt_{75}$ is unclear.[26] The theory predicts that $\mu_{Fe} = 3.25$ μ_B and $\mu_{Pt} = 0.38$ μ_B for $L1_2$ $Fe_{25}Pt_{75}$,[26] i.e., $\mu^*_{Fe} = 4.39$ μ_B, assuming ferromagnetic ordering. Therefore, the moment values of $A1$ and $L1_2$ $Fe_{25}Pt_{75}$ are comparable, with the latter about 18% larger. We note that bcc α-Fe has a magnetic moment of 2.27 μ_B. The high sensitivity of μ_{Fe} to the structure is due to the weak ferromagnetism nature of Fe,[27,28] in which the interatomic spacing plays an important role in the moment formation. Furthermore, our $A1$ $Fe_{29}Pt_{71}$ thin film is ferromagnetic at room temperature, whereas the $L1_2$ $Fe_{25}Pt_{75}$ is likely ferrimagnetic, if not antiferromagnetic.[26]

As the Fe concentration increases, μ^*_{Fe} reaches a peak value of 3.6 μ_B for $Fe_{35}Pt_{65}$. A simple moment mixing argument would yield μ^*_{Fe} of 3.3 μ_B and a monotonically *decreasing* μ^*_{Fe} with the Fe concentration. Most likely, the observed enhancement of the moment is due to the changing hybridization between the Fe 3*d* and the Pt 5*d* orbitals and between the *d* and *sp* orbitals.[29] The minority 3*d* band of Fe is nearly empty, while the majority of 3*d* of Fe and both 5*d* bands of Pt are filled. The maximum Fe moment could reach 4 μ_B, assuming little hybridization between the *d* and *sp* orbitals.[17,29] Including the $\mu_{Pt} = 0.3$ μ_B, the maximum μ^*_{Fe} is 4.6 μ_B at x = 35. The observed $\mu^*_{Fe} = 3.6$ μ_B in our $A1$ $Fe_{35}Pt_{65}$

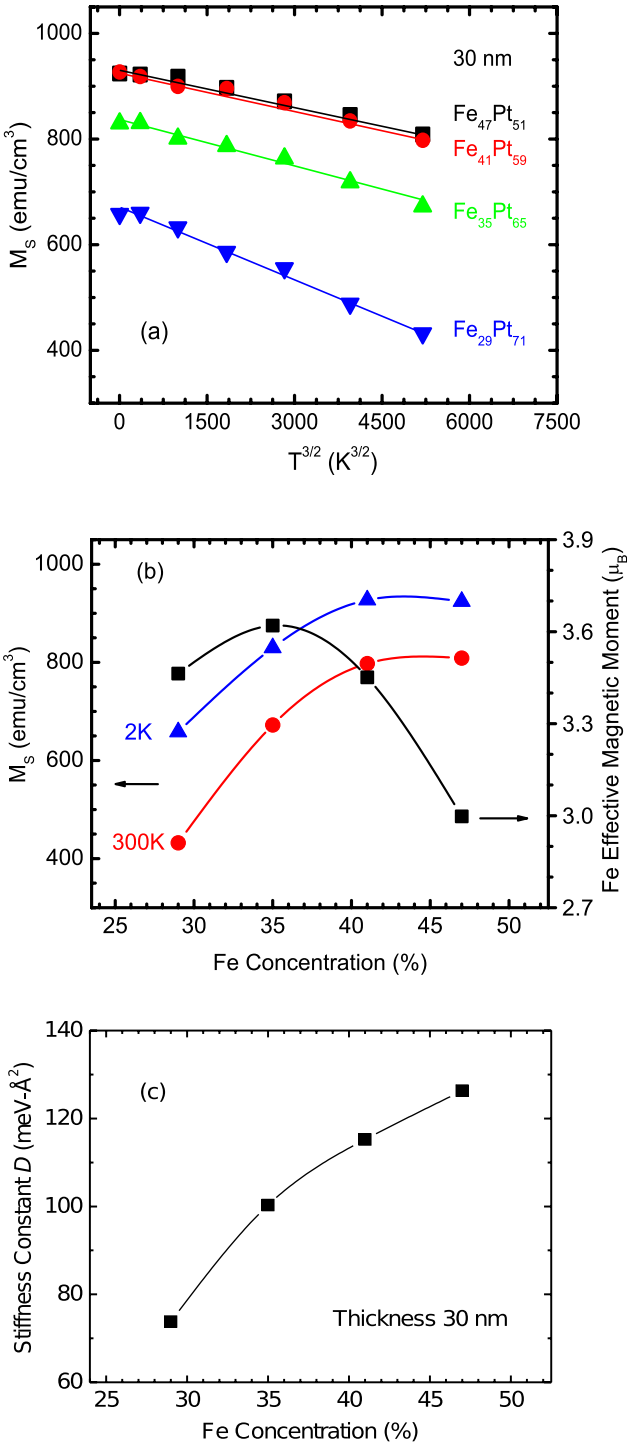

FIG. 3. (a) Spontaneous magnetization $M_S(T)$ versus $T^{3/2}$ to show the temperature dependence for Fe_xPt_{100-x} with the same thickness of 30 nm. (b) Fe concentration dependence of M_S(2 K), M_S(300 K) and Fe effective magnetic moment μ^*_{Fe} for the same series of the sample. The calculation of μ^*_{Fe} is based on the assumption that both the Fe and the induced Pt moment reside on Fe only. (c) Spin-wave stiffness constant *D* versus Fe concentration obtained from (a).

indicates that this alloy has not reached the unique situation of the fully occupied majority 3*d* state.

As shown in Fig. 3(b), beyond $Fe_{35}Pt_{65}$, the effective Fe moment decreases to $\mu^*_{Fe} = 3.0$ μ_B for $Fe_{47}Pt_{53}$, consistent with the simple moment mixing which predicts $\mu^*_{Fe} = 3.1$ μ_B. Following the trend line, we estimate that $\mu^*_{Fe} \approx 2.8$ μ_B for $A1$ $Fe_{50}Pt_{50}$, which is about 14% smaller than $\mu^*_{Fe} = 3.24$ μ_B

(μ_{Fe}= 2.83 μ_B and μ_{Pt}= 0.41 μ_B) for the $L1_0$ $Fe_{50}Pt_{50}$.[26] The intrinsic magnetic properties of the $L1_0$ $Fe_{50}Pt_{50}$ phase are T_C = 750 K, $M_S(300\,K) = 1140\,emu/cm^3$ and magnetic anisotropy constant $K_1 = 6.6 \times 10^7\,erg/cm^3$.[17,19] $L1_0$ $Fe_{50}Pt_{50}$ is a strong magnet,[17,19] whereas its $A1$ counterpart is a soft magnet. Overall, the magnetic moment formation in the $A1$ and super-structures of Fe-Pt is similar. However, the random and ordered structures differ significantly in magnetic ordering and anisotropy.

We study the temperature dependence of spontaneous magnetization by fitting Eq. (1) to the data in Fig. 3(a). According to the mean-field theory of ferromagnetism, the constant A which depends on the strength of the exchange interaction is given by

$$A = 2.612\left(\frac{V}{S}\right)\left(\frac{k_B}{4\pi D}\right)^{\frac{3}{2}}, \quad (2)$$

where D is the spin-wave stiffness constant, V is the volume per magnetic (Fe) atom which has a spin S, and k_B is the Boltzmann constant.[23] Based on Eq. (2), we calculate D which is shown in Fig. 3(c) as a function of Fe concentration. D steadily increases from 74 to 126 meV Å^2 as the Fe concentration increases from 29% to 47%, indicating the intensifying exchange interaction. In comparison, D = 307 meV Å^2 for bcc α-Fe.[30]

Next, we focus on the electron transport. We measure the resistivities ρ_{xx} of our Fe_xPt_{100-x} samples with different thicknesses over the temperature range of 2–300 K. The results are shown in Fig. 4(a). All samples share similar thermal ρ_{xx} behavior, i.e., decreasing ρ_{xx} as T is lowered. Fe_xPt_{100-x} solid solutions are characterized by high resistivities (~100 $\mu\Omega$ cm and above) at room temperature. Disordered electron scatterings dominate the electron transport as measured by the large residual resistivities. On average, the thermally induced ρ_{xx} caused by electron inelastic scatterings is about 25% of the residual ρ_{xx}(0 K). Therefore, in the Fe_xPt_{100-x} alloy system, ρ_{xx} is dominated by the elastic electron scatterings which can be caused by the disordered scatterings or spin-orbit scatterings.

Figure 4(b) shows the thickness dependence (1/t) of ρ_{xx}(300 K) for $Fe_{29}Pt_{71}$ from 1.4 to 30 nm. It is evident that ρ_{xx} scales linearly with 1/t, as expected from the finite-size effect of electron transport. In a metallic thin film, when t is larger than the effective electron mean free path λ_{eff}, the thin-film resistance can be expressed as[31]

$$\rho(t) = \rho_B + \frac{3}{8}\rho_B\lambda_{eff}/t, \quad (3)$$

where ρ_B is the bulk resistivity. The solid straight line in Fig. 4(b) is the fit of Eq. (3) to the resistivity data, yielding two fitting parameters $\rho_B(300\,K) = 98 \pm 1\,\mu\Omega\cdot cm$ and $\lambda_{eff}(300\,K) = 3.4 \pm 0.1$ nm. The bulk resistivity for $Fe_{29}Pt_{71}$ is large comparing with that of a typical metal at 300 K, e.g., ρ_B(Fe)=10.0 $\mu\Omega$ cm (Ref. 32) and ρ_B(Pt)=10.6 $\mu\Omega$ cm,[32] an indication that the $Fe_{29}Pt_{71}$ is a random alloy rich in disorder. The moderate value λ_{eff} allows us to vary the $\rho_{xx}(t)$ by nearly a factor 2 within our thickness range, which is beneficial to us in studying the correlation between the AHE and ρ_{xx} to be presented later.

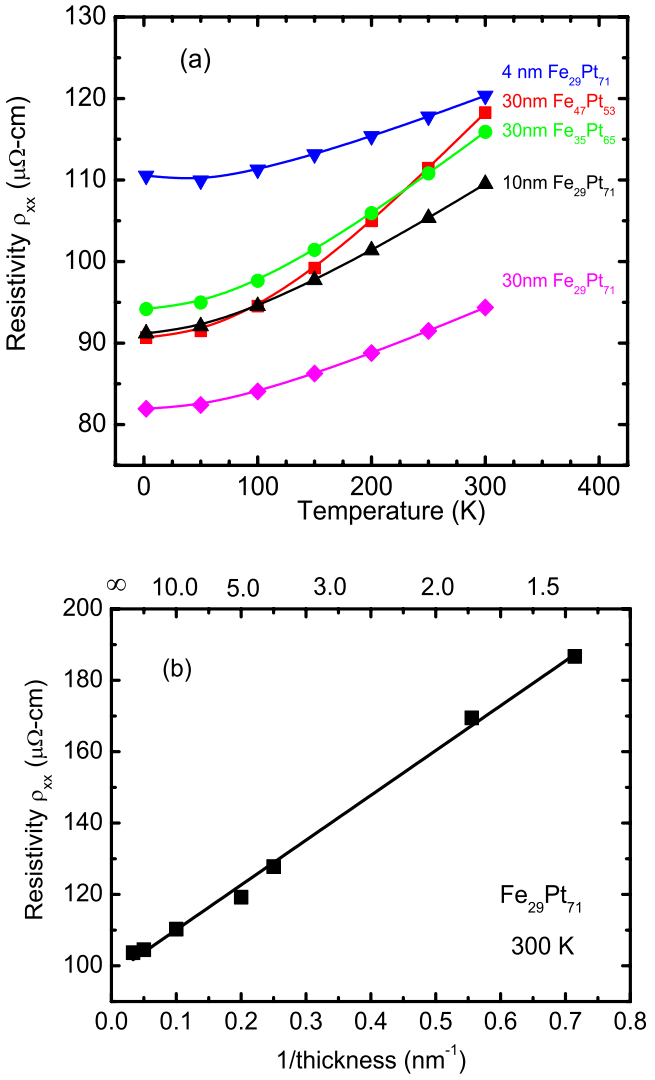

FIG. 4. (a) Temperature dependence of resistivity ρ_{xx} for Fe_xPt_{100-x} from 2 to 300 K. (b) Linear inverse thickness (1/t) dependence of resistivity ρ_{xx}(300 K) for $Fe_{29}Pt_{71}$, as a result of the finite-size effect of thin film resistivity.

Figure 5 shows the Hall resistivity ρ_{xy} as a function of magnetic field (up to ±2 T) for 5-nm $Fe_{29}Pt_{71}$ and 30-nm $Fe_{47}Pt_{53}$ within the temperature range of 2 to 300 K. The field is applied perpendicularly to the plane of the Hall bars. In a ferromagnetic metal, ρ_{xy} consists of two contributions,[1] the normal Hall effect and the AHE

$$\rho_{xy} = \rho_0 H + 4\pi R_S M_Z, \quad (4)$$

where ρ_0 is the normal Hall coefficient, R_s is the AHE coefficient, and M_z is the magnetization. In all our samples, the field dependent ρ_{xy} curves resemble the magnetic hysteresis curves closely. ρ_{xy} is dominated by the AHE and is proportional to M_z. As shown in Fig. 5, ρ_{xy} increases with the field linearly up to a saturation field (B^*), beyond which ρ_{xy} reaches a saturated value. This is because Fe_xPt_{100-x} alloys have in-plane (x-y) magnetic anisotropy, and the z-axis is the magnetic hard-axis. The largest saturated ρ^*_{xy} value that we obtain is 6.02 $\mu\Omega\cdot cm$

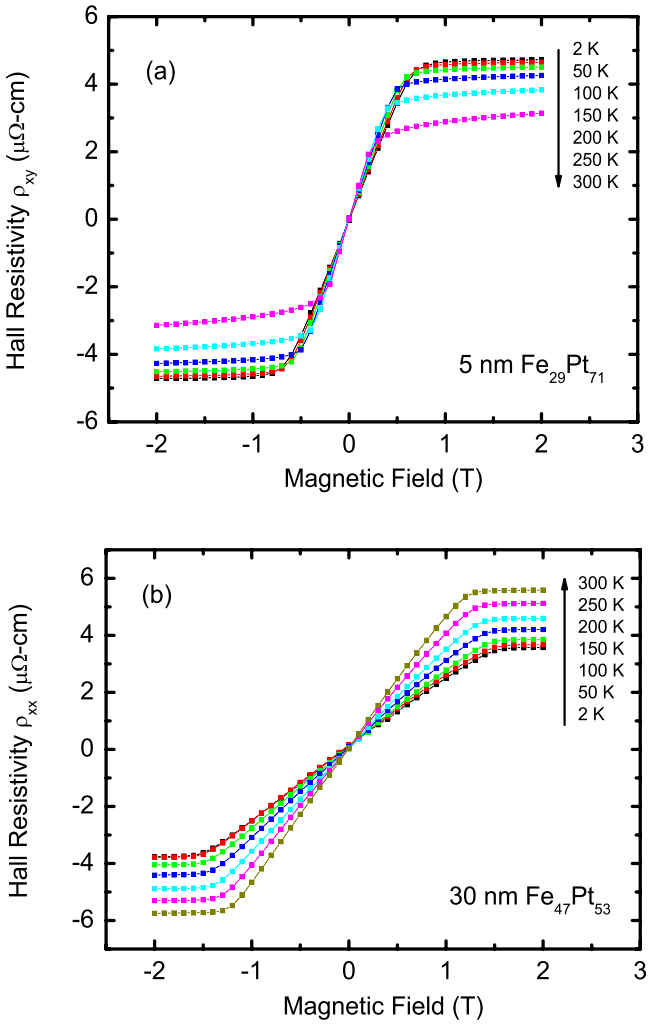

FIG. 5. Hall resistivity ρ_{xy} versus magnetic field from −2 to +2 T and measured at various temperatures from 2 to 300 K, for 5 nm-thick $Fe_{29}Pt_{71}$, and 30 nm-thick $Fe_{47}Pt_{53}$. The measurement current is 1 mA, and magnetic field is applied perpendicular to the film planes.

for the 30-nm thick $Fe_{41}Pt_{59}$ film at 300 K. As a comparison, the normal Hall coefficients for Pt and Fe are -0.24×10^{-2} and 0.25×10^{-2} $\mu\Omega$ cm/T, respectively.[33] In other words, at 1 T (approximately B^*), the normal Hall resistivities are -0.24×10^{-2} for Pt and 0.25×10^{-2} $\mu\Omega$ cm for Fe. Therefore, the AHE in Fe_xPt_{100-x} alloys is more than 3 orders of magnitude larger than their normal Hall effect. The large AHE in this system makes it an excellent candidate for use in solid state magnetic field sensors which are metal-based and nearly hysteresis-free.

Using the $\rho_{xx}(T)$ and $\rho^*_{xy}(T)$ data, we calculate the saturated Hall angle $\Theta(T)=\rho^*_{xy}(T)/\rho_{xx}(T)$, which is shown in Fig. 6 as a function of temperature for the Fe_xPt_{100-x} alloy system within the temperature range of 2 to 300 K. The maximum Θ is 0.059 at 2 K and 0.053 at 300 K for the 30 nm-thick $Fe_{29}Pt_{71}$ and $Fe_{35}Pt_{65}$ film, respectively. As a comparison, the recently discovered GSHE has shown that the spin Hall angle for pure Pt is 0.08.[33–36] Our Θ values for the Fe_xPt_{100-x} alloy system are lower, but comparable to that in pure Pt, due to a significant Fe concentration in Fe_xPt_{100-x} which may weaken the average spin-orbit coupling strength in the solids. We note

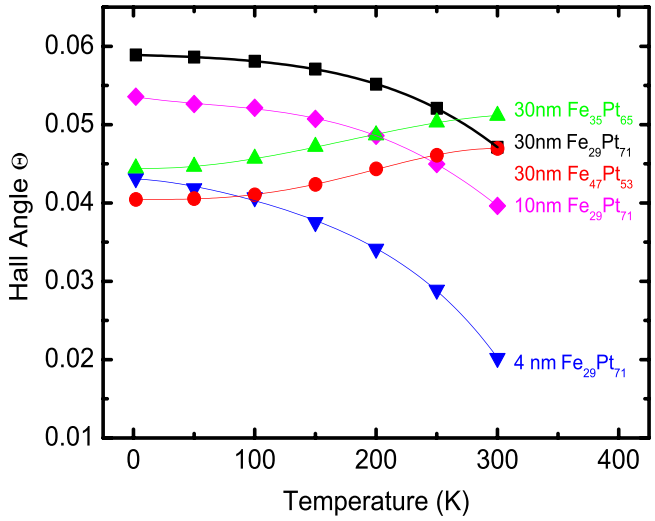

FIG. 6. Hall angle versus temperature from 2 to 300 K for a series of Fe_xPt_{100-x} films.

that β-Ta[4] and β-W[5,6,37] have Θ=0.15 and 0.40, respectively. Another interesting observation in Fig. 6 is that Θ for the $Fe_{29}Pt_{31}$ films decreases with the increasing temperature, but for films with higher Fe concentrations ($Fe_{35}Pt_{65}$, $Fe_{41}Pt_{59}$, and $Fe_{47}Pt_{53}$) Θ increases with temperature. The reason is that $\Theta(T)$ depends on three parameters $\rho_{xx}(T)$, $R_S(T)$, and $M_S(T)$. For different Fe concentrations, these three parameters change with temperature differently, hence, a different T-dependent $\Theta(T)$. It is anticipated that a film with concentration between $Fe_{29}Pt_{31}$ and $Fe_{35}Pt_{65}$ will yield a nearly T-independent Θ, a desirable property in applications. It is possible that the temperature dependent $\Theta(T)$ at different Fe concentrations may offer important clues in the theoretical investigation on the intrinsic mechanism of AHE.[1]

We also characterize the Hall angle for Fe_xPt_{100-x} films with different thicknesses. Figure 7 shows the thickness dependence of Θ at 300 K. Such a dependence can be explained by the finite spin diffusion length λ_{sf} in the films,[3] according to

$$\frac{\Theta(t)}{\Theta(\infty)} = 1 - \mathrm{sech}\left(\frac{t}{\lambda_{sf}}\right), \tag{5}$$

where $\Theta(\infty)$ is the Hall angle in the bulk limit. Due to the fluctuation of the data, the fitting quality is marginal. The extracted λ_{sf} is 3.9±0.2 nm. It is worth noting that λ_{sf} in the Fe_xPt_{100-x} system is larger than but comparable to the electron mean free path λ_{eff}= 3.4±0.1 nm determined earlier. Therefore, the electron scattering rate seems to be on the order of the spin flipping rate. As a comparison, in β-W films that are also characterized by strong SOI, λ_{sf} (β-W) = 3.5 nm[6] is about one order of magnitude larger than λ_{eff} (β-W) = 0.5 nm.[37] The bulk β-W sports a large spin Hall angle of nearly 0.4, which may be benefited from the large ratio of $\lambda_{sf}/\lambda_{eff}=7$.

The AHE is caused by the SOI in a ferromagnetic metal through intrinsic and extrinsic mechanisms.[1] The intrinsic Karplus-Luttinger mechanism is related to the Berry phase curvature,[1,7,8] whereas the extrinsic mechanisms are due to

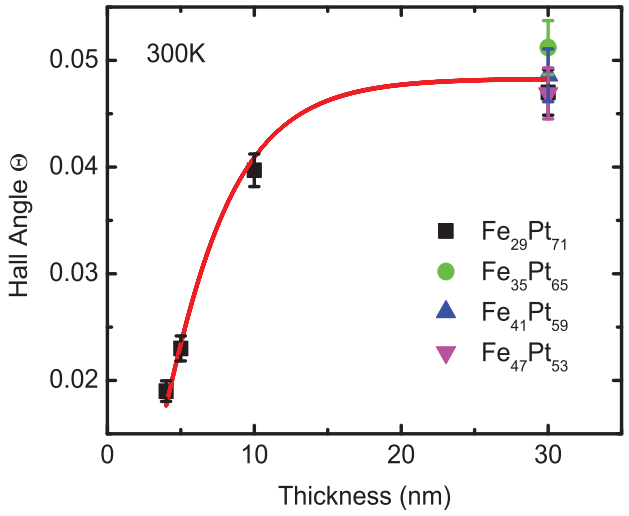

FIG. 7. Hall angle versus thickness for a series of Fe_xPt_{100-x} films. The line represents theoretical fitting to the data assuming a finite spin diffusion length in the films. The extracted λ_{sf} is 3.9±0.2 nm.

skew scattering or side jump at disorders[1] such as random sites, impurities, and grain boundaries. Typically, the relationship between AHE and longitudinal resistivity can be expressed as[1]

$$R_S = B \cdot \rho_{xx}^n, \tag{6}$$

where B is a constant and the exponent n is 1 due to skew scattering or 2 due to side jump or the intrinsic mechanism.[1] Separating the extrinsic side jump mechanism from the intrinsic mechanism is challenging. We calculate R_S based on Eq. (4) as follows:

$$R_S = \frac{\rho_{xy}^*}{4\pi M_S}, \tag{7}$$

where ρ_{xy}^* is the saturated AHE resistivity and M_S is the spontaneous magnetization which we measured earlier [see Fig. 3(a)]. Figure 8 shows a log-log plot of R_s versus ρ_{xx} for the Fe_xPt_{100-x} alloy system with different film thicknesses and compositions. Each straight line represents a particular composition with a given thickness. The hidden parameter behind each line is temperature which changes both R_s and ρ_{xx}. The slope of each line yields the exponent n in Eq. (6). Based on the data from all of our samples, we obtain $n = 1.93 \pm 0.14$. Therefore, the skew scattering is not dominant in the Fe_xPt_{100-x} system which is characterized by large resistivities (85–130 $\mu\Omega$ cm). Side jump should be dominant in this type of system; however, it is uncertain how much the intrinsic mechanism is at play.

Theoretical studies on the Fe_xPt_{100-x} system would be highly beneficial at this stage. The continuous variation in the Fe concentration will change the band structure gradually and consequently the intrinsic mechanism of the AHE. Furthermore, the temperature dependence of the Hall angle and magnetic properties provide important information for a comprehensive theoretical understanding of this large SOI alloy system.

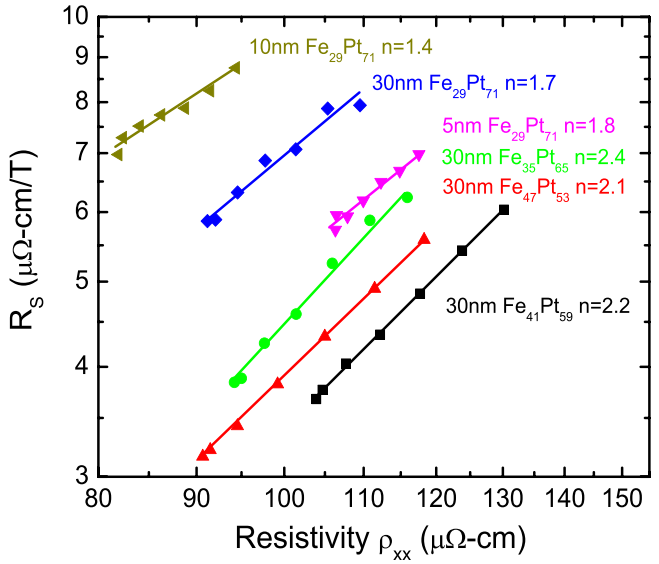

FIG. 8. Correlation between the anomalous Hall coefficient R_S and longitudinal resistivity ρ_{xx} in log-log scale for a series of Fe_xPt_{100-x} films. Straight lines represent the correlation of $R_S \sim \rho_{xx}^n$, with the exponent n being the slope of a line. The fitted n values for different samples are listed in the figure.

IV. CONCLUSIONS

In summary, we study magnetic properties, electron transport, and AHE of the $A1$ Fe_xPt_{100-x} thin films with different Fe concentrations ($29 \le x \le 47$ at. %), thicknesses ($1.8 \le t \le 30$ nm), and temperatures ($2 \le T \le 300$ K). The spontaneous magnetization of these ferromagnetic alloys is well described by Bloch's law of spin-wave excitation over the whole temperature range. The spin-wave stiffness constant increases monotonically with the Fe concentration as a result of the increasing magnitude of the exchange interaction. The Fe effective magnetic moment is enhanced with a peak value of 3.6 μ_B at $x = 35$. Due to the inherently strong spin-orbit interaction in the Fe_xPt_{100-x} system, the AHE is very large, more than 3 orders of magnitude stronger than the normal Hall effect. The maximum Hall angle is determined to be 0.06 at 2 K, and spin diffusion length is about 3.9±0.2 nm at 300 K. In comparison, the electron mean free path is determined to be 3.4±0.1 nm at 300 K. The correlation between the AHE and longitudinal resistivity reveals the dominance of the extrinsic side-jump mechanism and the intrinsic Karplus-Luttinger mechanism. However, we cannot distinguish the relative extrinsic and intrinsic contributions. This systematic study of the Fe_xPt_{100-x} system may elucidate theoretical understanding of the AHE in highly resistive metals and benefit applications in spintronics.

ACKNOWLEDGMENTS

We thank Cameron Reid for assistance. This work was supported by Nanoelectronics Research Initiative (NRI) through the Institute for Nanoelectronics Discovery and Exploration (INDEX) and by National Science Foundation through Grant No. DMR-1307056.

[1]N. Nagaosa, J. Sinova, S. Onoda, A. H. MacDonald, and N. P. Ong, "Anomalous Hall effect," Rev. Mod. Phys. **82**, 1539–1592 (2010).
[2]T. Seki *et al.*, "Giant spin Hall effect in perpendicularly spin-polarized FePt/Au devices," Nat. Mater. **7**, 125–129 (2008).
[3]L. Liu, T. Moriyama, D. C. Ralph, and R. A. Buhrman, "Spin-torque ferromagnetic resonance induced by the spin Hall effect," Phys. Rev. Lett. **106**, 036601 (2011).
[4]L. Liu *et al.*, "Spin-torque switching with the giant spin Hall effect of tantalum," Science **336**, 555–558 (2012).
[5]C.-F. Pai *et al.*, "Spin transfer torque devices utilizing the giant spin Hall effect of tungsten," Appl. Phys. Lett. **101**, 122404 (2012).
[6]Q. Hao and G. Xiao, "Giant spin Hall effect and switching induced by spin-transfer torque in a $W/Co_{40}Fe_{40}B_{20}/MgO/Ta$ structure with perpendicular magnetic anisotropy," Phys. Rev. Appl. **3**, 034009 (2015).
[7]R. Karplus and J. M. Luttinger, "Hall effect in ferromagnetics," Phys. Rev. **95**, 1154–1160 (1954).
[8]H. Kontani, T. Tanaka, and K. Yamada, "Intrinsic anomalous Hall effect in ferromagnetic metals studied by the multi-d-orbital tight-binding model," Phys. Rev. B **75**, 184416 (2007).
[9]T. Taniguchi, J. Grollier, and M. D. Stiles, "Spin-transfer torques generated by the anomalous Hall effect and anisotropic magnetoresistance," Phys. Rev. Appl. **3**, 044001 (2015).
[10]G. X. Miao and G. Xiao, "Giant Hall resistance in Pt-based ferromagnetic alloys," Appl. Phys. Lett. **85**, 73–75 (2004).
[11]Y. Zhu and J. W. Cai, "Ultrahigh sensitivity Hall effect in magnetic multilayers," Appl. Phys. Lett. **90**, 012104 (2007).
[12]M. Becherer *et al.*, "On-chip extraordinary Hall-effect sensors for characterization of nanomagnetic logic devices," Solid-State Electron. **54**, 1027–1032 (2010).
[13]Y. M. Lu, J. W. Cai, H. Y. Pan, and L. Sun, "Ultrasensitive anomalous Hall effect in SiO2/Fe-Pt/SiO2 sandwich structure films," Appl. Phys. Lett. **100**, 022404 (2012).
[14]I. Dubenko *et al.*, "Giant Hall effect in Ni-Mn-In Heusler alloys," Phys. Rev. B **80**, 092408 (2009).
[15]T. Zhu, P. Chen, Q. H. Zhang, R. C. Yu, and B. G. Liu, "Giant linear anomalous Hall effect in the perpendicular CoFeB thin films," Appl. Phys. Lett. **104**, 202404 (2014).
[16]O. A. Ivanov, L. V. Solina, V. A. Demshina, and L. M. Magat, "Determination of the anisotropy constant and saturation magnetization, and magnetic properties of powers of an iron-platinum alloy," Phys. Met. Metallogr. **35**, 81 (1973).
[17]J. Lyubina, "Nanocrysalline Fe-Pt alloys: Phase transformations, structure and magnetism," Ph.D. thesis (Leibniz Institute for Solid State and Materials Research Dresden, 2006).
[18]*Binary Alloy Phase Diagram*, edited by T. B. Massalski (ASM international, Ohio, 1990).
[19]M. H. Kryder *et al.*, "Heat assisted magnetic recording," Proc. IEEE **96**, 1810 (2008).
[20]B. Rellinghaus, J. Kästner, T. Schneider, E. F. Wassermann, and P. Mohn, "Thermodynamic analysis of $Fe_{72}Pt_{28}$ Invar," Phys. Rev. B **51**, 2983–2993 (1995).
[21]R. A. Ristau, K. Barmak, L. H. Lewis, K. R. Coffey, and J. K. Howard, "On the relationship of high coercivity and L10 ordered phase in CoPt and FePt thin films," J. Appl. Phys. **86**, 4527–4533 (1999).
[22]C. L. Canedy, G. Q. Gong, J. Q. Wang, and G. Xiao, "Large magnetic Hall effect in ferromagnetic FexPt100−x thin films," J. Appl. Phys. **79**, 6126–6128 (1996).
[23]D. C. Mattis, *Theory of Magnetism* (Harper and Row, 1965).
[24]M. D. Kuz'min, "Shape of temperature dependence of spontaneous magnetization of ferromagnets: Quantitative analysis," Phys. Rev. Lett. **94**, 107204 (2005).
[25]A. Z. Menshikov, Y. A. Dorofeev, V. A. Kazanzev, and S. K. Sidorov, "Magnitnaya struktura uporyadochennih zhelezoplatinovih splavov," Fiz. Metall. Metalloved. **38**, 505–518 (1974).
[26]S. O. Ponomaryova, V. A. Tatarenko, Y. M. Koval, V. V. Odnosum, and O. P. Ponomaryov, "Magnetic interactions in F.C.C. Fe–Pt alloys," Int. J. Mech. Mater. Eng. **3**, 45–53 (2014).
[27]F. J. Pinski, J. Staunton, B. L. Gyorffy, D. D. Johnson, and G. M. Stocks, "Ferromagnetism versus antiferromagnetism in face-centered-cubic iron," Phys. Rev. Lett. **56**, 2096–2099 (1986).
[28]G. Xiao and C. L. Chien, "Nonuniqueness of the state of amorphous pure iron," Phys. Rev. B **35**, 8763–8766 (1987).
[29]G. H. O. Daalderop, P. J. Kelly, and M. F. H. Schuurmans, "Magnetocrystalline anisotropy and orbital moments in transition-metal compounds," Phys. Rev. B **44**, 12054–12057 (1991).
[30]C. K. Loong, J. M. Carpenter, J. W. Lynn, R. A. Robinson, and H. A. Mook, "Neutron scattering study of the magnetic excitations in ferromagnetic iron at high energy transfers," J. Appl. Phys. **55**, 1895–1897 (1984).
[31]L. Eckertova, *Physics of Thin Films* (Plenum, 1986), pp. 219–233.
[32]R. A. Serway, *Principles of Physics* 2nd ed. (Saunders College Pub, 1998), p. 602.
[33]A. Azevedo, L. H. Vilela-Leão, R. L. Rodríguez-Suárez, A. F. Lacerda Santos, and S. M. Rezende, "Spin pumping and anisotropic magnetoresistance voltages in magnetic bilayers: Theory and experiment," Phys. Rev. B **83**, 144402 (2011).
[34]N. Vlietstra *et al.*, "Exchange magnetic field torques in YIG/Pt bilayers observed by the spin-Hall magnetoresistance," Appl. Phys. Lett. **103**, 032401 (2013).
[35]O. J. Lee *et al.*, "Central role of domain wall depinning for perpendicular magnetization switching driven by spin torque from the spin Hall effect," Phys. Rev. B **89**, 024418 (2014).
[36]A. Ganguly *et al.*, "Thickness dependence of spin torque ferromagnetic resonance in Co75Fe25/Pt bilayer films," Appl. Phys. Lett. **104**, 072405 (2014).
[37]Q. Hao, W. Chen, and G. Xiao, "Beta (β) tungsten thin films: Structure, electron transport, and giant spin Hall effect," Appl. Phys. Lett. **106**, 182403 (2015).